Visible and near infrared spectroscopic investigation of E-type asteroids, including 2867 Steins, a target of the Rosetta mission

S. Fornasier, A. Migliorini, E. Dotto, M.A. Barucci

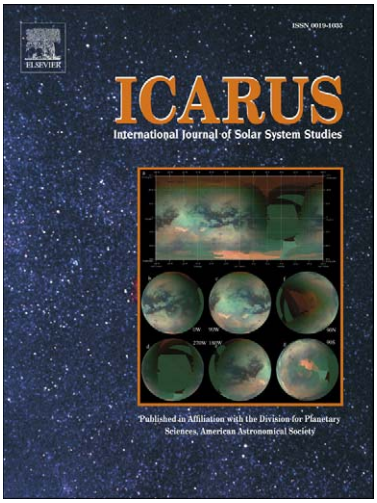

Visible and near infrared spectroscopic investigation of E-type asteroids, including 2867 Steins, a target of the Rosetta mission

S. Fornasier, A. Migliorini, E. Dotto, M.A. Barucci

PII: S0019-1035(08)00104-8
DOI: 10.1016/j.icarus.2008.02.015
Reference: YICAR 8619

To appear in: *Icarus*

Received date: 10 October 2007
Revised date: 26 February 2008
Accepted date: 28 February 2008

Please cite this article as: S. Fornasier, A. Migliorini, E. Dotto, M.A. Barucci, Visible and near infrared spectroscopic investigation of E-type asteroids, including 2867 Steins, a target of the Rosetta mission, *Icarus* (2008), doi: 10.1016/j.icarus.2008.02.015

Visible and near infrared spectroscopic investigation of E-type asteroids, including 2867 Steins, a target of the Rosetta mission*

S. Fornasier[1,2], A. Migliorini[3], E. Dotto[4], M.A. Barucci[1]

March 7, 2008

[1] LESIA, Observatoire de Paris, 5 Place Jules Janssen, F-92195 Meudon Principal Cedex, France

[2] Université de Paris 7 *Denis Diderot*, 4, rue Elsa Morante 75205 PARIS CEDEX 13, France

[3] IASF-INAF, via del Fosso del Cavaliere 100, 00133 Roma, Italy

[4] INAF, Osservatorio Astronomico di Roma, via Frascati 33, I-00040 Monteporzio Catone (Roma), Italy

Submitted to Icarus: October 2007

e-mail: sonia.fornasier@obspm.fr; fax: +33145077144; phone: +33145077746

Manuscript pages: 52; Figures: 18; Tables: 2

*Based on observations carried out at the European Southern Observatory (ESO), La Silla, Chile, ESO proposal 074.C-0049 and 078.C-0115 and at the Telescopio Nazionale Galileo

Running head: Investigation of E-type asteroids

Send correspondence to:

Sonia Fornasier

LESIA-Observatoire de Paris

Batiment 17

5, Place Jules Janssen

92195 Meudon Cedex

France

e-mail: sonia.fornasier@obspm.fr

fax: +33145077144

phone: +33145077746

Abstract

We present the results of a visible spectroscopic and photometric survey of igneous asteroids belonging to the small and intriguing E-class, including 2867 Steins, a target of the Rosetta mission. The survey was carried out at the 3.5m Telescopio Nazionale Galileo (TNG), and at the 3.5m New Technology Telescope (NTT) of the European Southern Observatory.

We obtained new visible spectra for eighteen E-type asteroids, and near infrared spectra for eight of them. We confirm the presence of three different mineralogies in the small E-type populations. We classify each object in the E[I], E[II] or E[III] subgroups (Gaffey & Kelley, 2004) on the basis of the spectral behavior and of the eventual presence of absorption features attributed to sulfides (such the 0.49 μm band, on E[II]), or to iron bearing silicates (0.9 μm band, on E[III]).

We suggest that some asteroids (i.e. 64 Angelina, 317 Roxane, and 434 Hungaria), which show different spectral behavior comparing our data with those available in literature, have an inhomogeneous surface composition. 2867 Steins, a target of the Rosetta mission, shows a spectral behavior typical of the E[II] subgroup, as already suggested by Barucci et al. (2005) and Fornasier et al. (2007).

Litva and 1990 TN1, initially classified as E-types, show a visible and near infrared behavior consistent with the olivine rich A-class asteroids, while 5806 Archieroy, also supposed to belong to the E-class, has a spectral behavior consistent with the S(V) classification following the Gaffey et al. (1993) classification scheme.

To fully investigate the E-type population, we enlarged our sample including 6 E-type asteroids spectra available in literature, resulting in a total sample of 21 objects. The analysis of the spectral slope for the 3 different E-type subgroups versus the orbital elements show that E[III] members have the lowest mean spectral slope value inside the whole sample, and that they are located between 2.2-2.7 AU in low inclination orbits. E[II] members has the highest spectral slope inside the sample, half of them are located in the Hungaria region, 2 are NEA and 2 (64 Angelina and 2867 Steins), are in the main belt. A similar distribution is found for the 5 featureless E[I] members, located mainly in the Hungaria region (3 members), one in the middle main belt while one is a NEA (2004 VD17).

Finally, for the five E-type asteroids observed both in the visible and near infrared range, plus 2867 Steins, we attempt to model their surface composition using linear geographycal mixtures of no more than 3 components, selected from aubrite meteorites and correlated minerals. In particular we suggest that the aubrite Peña Blanca might have the E[III] asteroid 317 Roxane as parent body, and that the aubrite ALH78113 might be related to the E[II] subgroup asteroids.

keywords: Asteroids, surface – Spectroscopy

1 Introduction

The E-type asteroids are a small population which comprises around 25 asteroids to date. These bodies are called igneous as they formed and differentiated under relatively reducing conditions, with parent bodies heated to at least 1580 $°C$ (Keil, 1989). The population is dynamically concentrated into 2 groups, located respectively in the Hungaria region, around 1.9 AU, and in the inner part of the main belt, between 2.1 and 2.7 AU. In addition, some Near Earth Asteroids were recognized to belong to the E-class (Deluise et al., 2007; Delbo et al. 2003; Harris et al. 2007).

E-type asteroids were grouped, together with M– and P–type, in the X–type complex following Tholen (1989) taxonomic system. They have the highest albedo than any other asteroids class (around 0.4–0.6).

Their surface composition seems to be dominated by iron-free or iron-poor silicates such as enstatite, forsterite or feldspar, and they are thought to be the parent bodies of the aubrite (enstatite achondrites) meteorites (Gaffey et al. 1989, Gaffey et al., 1992, Zellner et al., 1977). Initially, E-type asteroids were believed to have a quite flat or slightly reddish featureless spectral behavior (Tholen, 1989), but, since 1995, some absorptions bands, both in the visible and near infrared region, were identified on their surface: a very sharp absorption band, until now observed only for these bodies, centered at 0.49-0.50 μm, extended from 0.43 to 0.55 μm, (Burbine et al., 1998, Fornasier & Lazzarin, 2001; Bus & Binzel, 2002a; Clark et al., 2004), attributed to the presence of sulfides (known constituent of the aubrite meteorites) such as

oldhamite; two weaker features centered at around 0.9 μm and 1.8 μm attributed to iron bearing pyroxene such as orthopyroxene or forsterite (Clark et al., 2004); an absorption feature at 3 μm (Rivkin et al., 1995), typically associated with the first overtone of H_2O and with OH vibrational fundamentals on hydrated silicates, not expected on highly evolved bodies like the E-type asteroids. After the discovery of these absorptions features, 3 different mineralogies have been suggested to be present inside the E-type population (Clark et al., 2004; Gaffey & Kelley, 2004). Following the Gaffey & Kelley (2004) classification scheme, we observe 3 subgroups, named E[I], E[II] and E[III]. E[I] asteroids do not present absorption features, but a slightly reddish slope in the visible spectral range; this spectral behavior is characteristic of aubritic pyroxene plus feldspar assemblage. E[I] asteroids might be the parent bodies of the aubrite meteorites. The parent bodies of the E[I] subgroup attained temperatures in excess of 1400^oC (McCoy et al., 1999).

The subgroup E[II] presents the strong absorption at ~ 0.49 μm and occasionally at 0.90–0.96 μm. These features are possibly due to the calcium sulfide mineral oldhamite (present in highly reduced assemblages such as aubrites). The typical example of the E[II] subgroup is 64 Angelina. These bodies are probably composed of basalt equivalents from enstatite chondrite-like parent bodies which underwent at least partial melting (Gaffey & Kelley, 2004).

Finally, E[III] are characterized by a flat or reddish spectral curve with a well defined band centered at $0.89 - 0.9\mu$m, due to enstatite pyroxene containing Fe^{2+}. Some of the asteroids having the 0.9 μm band shows an absorption feature also at 1.8 μm (Clark et al., 2004). 44 Nysa is a typical member of

this subclass. The asteroids of this subgroup are supposed to be derived from oxidized parent bodies which underwent extensive reduction during their igneous processing (Gaffey & Kelley, 2004).

An exhaustive discussion on the E–type asteroids composition and classification throughout different taxonomic schemes is reported in Clark et al. (2004), and in Gaffey & Kelley (2004).

Since 2004 we have carried out a spectroscopic survey in the visible and near infrared range of E-type asteroids at the 3.5m Telescopio Nazionale Galileo (TNG), La Palma, Spain, and at the 3.5m New Technology Telescope (NTT) of the European Southern Observatory, La Silla, Chile. The aim is to extend the spectral analysis to a larger number of E-type asteroids, investigate their surface properties throughout the rotational period and define the mineralogical properties of each sub-group. We obtained new spectra on 18 asteroids previously classify as E-type asteroids, that is more than 2/3 of the known population. These data, together with those already published in literature, draw a representative picture of the spectral properties of this peculiar class of asteroids.

2 Observations and data reduction

The data presented in this work were obtained during 2 runs (February and November 2004) at the TNG telescope, and during 3 runs (May 2004, August 2005, and January 2007) at the NTT telescope. We get a total of 11 observing nights devoted to the investigation of asteroids belonging to the

E, M and X taxonomic classes. Here we present the results of our E-type observations.

At the TNG telescope, for visible spectroscopy we used the DOLORES (Device Optimized for the LOw RESolution) instrument equipped with the low resolution red grism (LR-R) covering the 0.51–0.95 μm range with a spectral dispersion of 2.9 Å/px. Most part of the objects were observed also with the low resolution blue grism (LR-B, dispersion of 2.8 Å/px) on February 2004, covering the 0.38-0.80 μm range, and with the medium resolution blue grism (MR-B, dispersion of 1.7 Å/px, 0.38-0.70 μm range), for the November 2004 run. The 'red' and 'blue' spectra in the visible range were separately reduced and finally combined together to obtain a spectral coverage from 0.38 to 0.95 μm. The DOLORES detector is a Loral thinned and back-illuminated CCD with 2048 $\times$ 2048 pixels, with a pixel size of 15 μm and a pixel scale of 0.275 arcsec/px. Like most of the Loral CCDs, that of DOLORES is affected by moderate-to-strong fringing at red wavelengths. Despite taking as much care as possible in the data reduction, for two asteroids (317 Roxane and 2048 Dwornik) we get a lot of fringing residuals and we were obliged to cut their spectra for wavelengths longer than $\sim$ 0.8 μm.

For the infrared spectroscopic investigation at the TNG telescope we used the near infrared camera and spectrometer (NICS) equipped with an Amici prism disperser. This equipment covers the 0.85–2.40 μm range during a single exposure with a spectral resolution of about 35. The detector is a 1024 $\times$ 1024 pixel Rockwell HgCdTe Hawaii array.

The spectra were acquired nodding the objects along the spatial direction

of the slit, in order to obtain alternated pairs (named A and B) of near–simultaneous images for the background removal. Both for the visible and near infrared observations we utilized a 1.5 arcsec wide slit, oriented along the parallactic angle to minimize the effect of atmospheric differential refraction.

At the NTT telescope, the visible spectra were acquired using the EMMI instrument, equipped with a 2x1 mosaic of 2048×4096 MIT/LL CCD with square 15μm pixels. We used the grism #1 (150 gr/mm) in RILD mode to cover the wavelength range 4100–9600 Å with a dispersion of 3.1 Å/px at the first order.

For the near infrared spectroscopy, we utilized the instrument SOFI (Son OF Isaac) in the low resolution mode. The blue and red grisms, covering respectively the 0.95–1.64 μm (dispersion of 6.96 Å/px) and the 1.53–2.52 μm range (dispersion of 10.22 Å/px) were used. The acquisition technique was identical to that explained for the TNG observations, except the slit was wider (2 arcsec) but always oriented along the parallactic angle. The two parts of the blue and red grisms observations were combined matching the overlapping region in the 1.53–1.64 μm range.

The visible and near infrared spectra were reduced using ordinary procedures of data reduction with the software packages Midas and IDL as described in Fornasier et al. (2004a,b). For the visible spectra, the procedure includes the subtraction of the bias from the raw data, flat–field correction, cosmic rays removal, sky subtraction, collapsing the two–dimensional spectra to one dimension, wavelength calibration and atmospheric extinction correc-

tion. The reflectivity of each asteroid was obtained by dividing its spectrum by that of the solar analog star closest in time and airmass to the object. Spectra were finally smoothed with a median filter technique, using a box of 19 pixels in the spectral direction for each point of the spectrum. The threshold was set to 0.1, meaning that the original value was replaced by the median value if the median value differs by more than 10% from the original one.

For the observations in the infrared range, first, spectra were corrected for flat fielding, then bias and sky subtraction was performed by producing A-B and B-A frames. Then, the positive spectrum of B-A frame was shifted and added on the positive spectrum of A-B frame. The final spectrum is the result of the mean of all pairs of frames previously combined. The spectrum was then extracted and wavelength calibrated. For the NTT-SOFI spectra, this last step was performed acquiring the spectrum in the blue and red grisms of a Xenon lamp, and comparing the observed line with those of a reference table, obtaining the dispersion relation. For the TNG-NICS spectra, due to the very low resolution of the Amici prism, the lines of Ar/Xe lamps are blended and cannot be easily used for standard reduction procedures. For this reason, the wavelength calibration was obtained using a look-up table which is based on the theoretical dispersion predicted by ray-tracing and adjusted to best fit the observed spectra of calibration sources. Finally, the extinction correction and solar removal was obtained by division of each asteroid spectrum by that of the solar analog star closest in time and airmass to the object. The stellar and asteroid spectra were cross-correlated and, if necessary, sub-pixel shifts

were made before the asteroid-ratio star division was done. This reduction step is needed to reduce the noise and/or the changes in the final asteroid slope due to small changes in the wavelength dispersion between asteroid and star observations, introduced by instrumental flexure.

The infrared and visible range spectra of each asteroid were finally combined overlapping the spectra, merging the two wavelength regions at the common wavelengths and utilizing the zone of good atmospheric transmission to find the normalization factor between the two spectral parts. For the TNG data the overlapping region goes from 0.88 to 0.94 μm, and we took the average value over the 0.89-0.91 micron region of the visible spectrum to normalize the infrared one. For the NTT data, considering that the overlapping region is very small (0.95-0.96 μm) we use curve fitting at the ends of each spectral part to extrapolate to the beginning of the next spectral region and to overlap the data. The spectra of the observed asteroids, all normalized at 0.55 μm, are shown in Figs. 1–16. The conditions of the observations are reported in Table 1.

[HERE TABLE 1]

3 Results

We investigated 16 out of the 23 known E-type asteroids listed in Clark et al. (2004, see Table 1) plus 2867 Steins, a target of the Rosetta mission, and 437 Rhodia, that were classified as E-types (Barucci et al., 2005). Eight of them were investigated both in the visible and near infrared range. We obtained

the first spectroscopic observations for 8 E-type asteroids listed in Clark et al. (2004), discovering that 3 of them (2577 Litva, 5806 Archieroy, and 7579 1990TN1), never observed before, show a spectral behavior in the visible and near infrared region that is not consistent with the E-type classification.

In the following subsections we discuss the spectral properties of each of the investigated asteroids, and we attempt to classify each of them into the 3 different subgroups proposed for the E-class, using the Gaffey & Kelley (2004) classification scheme, that we described previously. We also evaluate the spectral slope in 3 different wavelength regions (4900-5500 Å ($S1$), 5500–8000 Å ($S2$), and 8000–9000 Å ($S3$)), using a standard least squared technique. The spectral slope values (see Table 2) help us identify of the subgroup memberships. Asteroids belonging to the E[II] subgroup usually have a large value of the $S1$ slope (steep rise of the 0.49 μm band), while asteroids belonging to the E[III] subgroup have negative or very small values of the $S3$ slope (indicative of the presence of the absorption band centered at around 0.9 μm). For a more complete analysis, we include in Table 2 the spectral slope values for 6 E-type asteroids (1025 Riema, 2035 Stearn, 3050 Carrera, 3103 Eger, 4660 Nereus, 144989 2000VD17) not presented here but whose spectra are available in literature (Bus & Binzel, 2002a, Fornasier & Lazzarin (2001), Barucci et al., 2005; De Luise et al., 2007; Fornasier et al., 2007).

[HERE TABLE 2]

3.1 44 Nysa

44 Nysa is a main belt asteroid located at 2.42 AU. It has an albedo of 0.55±0.07 (Tedesco et al., 2002), a diameter of 71 km and a rotational period of 6.42 hours.

We get a full V+NIR spectrum of Nysa at the NTT telescope during Aug. 2005, plus 2 additional visible spectra obtained at the NTT (Jan. 07) and TNG telescopes (Feb. 04). All the spectra show an absorption band (Fig. 1) centered at ~ 0.9 μm, that appears to be deepest in the Jan 07 spectrum, as can be seen comparing the $S3$ slope in Table 2. The NIR spectrum indicates the presence of a broad absorption feature at ~ 1.8 μm, confirming the detection already reported by Clark et al. (2004). 44 Nysa is the archetype of the E[III] subgroup, with both the 0.9 and 1.8 μm absorption band indicative of iron bearing pyroxene such as orthopyroxene or forsterite.

The visible spectra shows slight differences in the spectral slopes evaluated in the 5500-8000 Å region, with the Feb. 04 spectrum being the steeper one. We also identify on the Aug. 05 spectrum a very faint band (depth $\sim 1.2\%$ as compared to the continuum) centered at 0.433 micron, wide around 0.02 μm. Due to its faintness, the detection of this band needs to be confirmed. If real, the band is not easily attributable: it might be associated to chlorites and Mg-rich serpentines, as suggested by King & Clark (1989) on enstatite chondrites; to pyroxenic minerals such us pigeonite or augite as suggested by Busarev (1998) on M-asteroids; or to an Fe^{3+} spin-forbidden transition in the iron sulfate jarosite, as suggested by Vilas et al. (1993) on low-albedo asteroids. Rivkin et al. (1995) detected the 3 micron absorption band on 44

Nysa and they suggested that it can be attributed to the presence of hydrated phases on its surface. Our detection of the 0.43 μm band, if it is really due to the presence of chlorites– Mg rich serpentines and/or to jarosite, might support this interpretation as these minerals are aqueous alteration products.

[HERE FIGURE 1]

3.2 64 Angelina

64 Angelina is located in the main belt, at 2.68 AU. It is the second largest E-type asteroid, after Nysa, with a diameter of about 60 km and an albedo of 0.43 (Tedesco et al., 1989). We obtained new visible and near infrared spectroscopic observations of 64 Angelina (Fig. 2) on November 2004, at the TNG telescope. The visible spectrum clearly shows the presence of the sharp absorption band centered at $\sim$ 0.492 μm, with a FWHM of 0.055 μm and a depth of about 8 %, probably due to the presence of oldhamite. Similar parameters for this absorption band were reported also by Fornasier & Lazzarin (2001), and the presence of the band confirmed by Burbine et al., (1998) and Clark et al. (2004). In addition, our spectrum clearly shows an absorption feature centered at 0.431 μm, with a width around 0.019 μm and a depth of $\sim$ 2% as compared to the continuum. This feature is similar to the aforementioned but fainter one detected on 44 Nysa, and, once again, if it is due to aqueous alteration products such as chlorites, serpentines or jarosite, it might support the hypothesis of the presence of hydrated phased on Angelina, as suggested by Rivkin et al. (1995) who observed the 3 micron band on its spectrum.

We do not have evidence on our spectrum of a shallow absorption feature at 0.92 μm reported by Burbine et al. (1998) and Clark et al. (2004). Our near infrared spectrum has a spectral behavior slightly reddish and different than that published by Clark et al. 2004. The difference could be associated with different rotational phases seen in the two observations (Angelina's rotational period is 8.75 hours), and could indicate some inhomogeneities on the surface of 64 Angelina.

Because of the sharp 0.49 μm band absorption, Angelina belongs to the E[II] sub-type.

[HERE FIGURE 2]

3.3 214 Aschera

214 Aschera has a semimajor axis of 2.61 AU, an IRAS albedo of 0.52±0.05 (Tedesco et al., 2002) and a diameter of 23 km. We obtained new data on two different runs at the NTT (May 04, visible spectrum) and TNG (Nov. 04, IR spectrum) telescopes. The spectrum shows the presence of a sharp band centered at 0.9 μm; in addition, there is an indication of a possible feature at $\sim$ 1.8 μm (Fig. 3), even though our spectrum has been cut in this region for the telluric bands residuals. These two bands were both detected by Clark et al. (2004) on their spectra. Using literature data from SMASS survey, Gaffey & Kelly (2004) classified Aschera as an E[I] subgroup member, due to the lack of any discrete disagnostic mineral absorption features. Nevertheless, the presence of the 0.9 and 1.8 μm spectral bands, independently detected by Clark et al. (2004) and in this work, confirms that 214 Aschera is a

Nysa–like object, and so it can be placed into the E[III] subgroup.

[HERE FIGURE 3]

3.4 317 Roxane

317 Roxane has a semimajor axis of 2.29 AU, an IRAS albedo of 0.49±0.08 (Tedesco et al., 2002) and an estimated diameter of $\sim$ 19 km. We acquired four new visible spectra and one in the infrared region using both the NTT and TNG telescopes (Fig 4). All the three visible spectra obtained at the NTT telescope show the 0.9 μm band, despite there are some variations in the shape within the different data set. The visible spectrum obtained at the TNG telescope does not give information on this absorption as it was cut at 0.81 μm, because of the fringing problems. The TNG spectrum also has a higher spectral slope value in the 5500-8000 Å region compared to the NTT spectra (Table 2). It also shows a drop off of the reflectance for wavelength $<$ 5200 Å that is similar to the behavior of the Jan. 07 spectrum, but different from the 2 spectra acquired on Aug. 05.

The Jan. 07 spectrum shows also a faint absorption centered at 0.51 μm, seen also on some M-type asteroids (Busarev, 1998; 2002) and possibly attributed to Fe^{2+} spin forbidden charge field transitions in pyroxenes.

The IR spectrum shows the 0.9 μm feature together with a faint absorption at 1.8 μm. Clark et al. (2004) present a spectrum which, in the infrared region, is different from the one we present here: it shows the 0.9 μm band and the 1.8 μm band, but there is a steep decrease in the spectral slope in the 1.3–1.9 μm range, while our spectrum has a gently reddish behavior. The

variation in the spectral behavior of 317 Roxane in our data and those coming from the literature can be attributed to some inhomogeneities in the surface composition of the asteroid, that has a rotational period of 8.17 hours. Due to the presence of the 0.9 and 1.8 μm bands, 317 Roxane is then classified as a E[III] subgroup member. Additional observations covering the whole rotational period of this object are needed to fully investigate its surface composition.

[HERE FIGURE 4]

3.5 434 Hungaria

434 Hungaria is located just outside the inner edge of main belt, at a semi-major axis of 1.94 AU. We get a spectrum only in the visible range that shows a faint absorption band centered at $\sim$ 0.49 micron, and a feature beyond 0.89 μm. Burbine et al (1998) and Bus & Binzel (2002a) also reported the presence of two absorption bands at 0.49 μm and 0.92 μm on their Hungaria spectrum. Nevertheless, in the Bus & Binzel (2002a) spectrum, the reflectance has a maximum at $\sim$ 0.75 μm and then decreases, while in our spectrum the reflectance has a red linear slope up to 0.89 μm. The visible spectra presented by Sawyer (1991) and Kelley & Gaffey (2002) do not shown the 0.9 μm band, while this absorption is clearly present in the infrared spectrum of Clark et al. (2004). 434 Hungaria, that has a long rotational period of 26.5 hours, shows different spectral behaviors that can be associated with some inhomogeneities in the surface composition. Due to the presence of the 0.5 μm band we classify Hungaria as a member of the E[II] subgroup.

[HERE FIGURE 5]

3.6 437 Rhodia

437 Rhodia is the asteroid with the highest albedo (0.70±0.08) in the IRAS dataset (Tedesco et al. 2002). It has a semimajor axis of 2.38 AU and an estimated diameter of 13 km. The first visible and near infrared spectrum of Rhodia was obtained by Barucci et al. (2005), who suggests a possible E-type classification on the basis of its high albedo and of its spectral behavior, which is similar to that of 44 Nysa. We obtained new spectra of Rhodia (Fig. 6) which clearly show both the 0.9 ad 1.8 μm bands, already reported by Barucci et al. (2005). The spectral behavior, together with the high albedo value, allow us to definitively classify Rhodia as an E-type asteroids, and in particular as a member of the E[III] subgroup. As compared to the two infrared spectra reported by Barucci et al. (2005, see their Fig. 2), that are slightly different beyond 1.4 μm, our IR spectrum is similar to first one (named a) they obtained.

[HERE FIGURE 6]

3.7 504 Cora

504 Cora was suggested to be an E-type asteroid by Clark et al. (2004) on the basis of the IRAS albedo (0.34, Tedesco et al. (2002)) and of the X classification given by Bus & Binzel (2002a). It is located in the middle of the main belt (semimajor axis of 2.72 AU) in an orbit with an eccentricity of 0.217. We observed Cora twice in visible spectroscopy both at the TNG and NTT telescopes, on February 2004 and August 2005 respectively (Fig. 7).

The 2 spectra have a very similar featureless linear reddish behavior.

Due to the absence of any absorption feature, 504 Cora might be classified as an E[I] subgroup member.

[HERE FIGURE 7]

3.8 620 Drakonia

We present the first spectroscopic observations, only in the visible range, of 620 Drakonia, a main belt asteroid with a semimajor axis of 2.43 AU and a rotational period of 5.48 hours. The spectrum, obtained at the NTT telescope on Jan. 07 (Fig. 8), is featureless and reddish from 0.45 to 0.77 μm, and it has a shallow broad absorption feature (depth of 1.4%) centered at around 0.9 μm. Unfortunately, we do not have any IR data so it is not possible to independently confirm the presence of the 0.9 μm band. The visible spectrum of Drakonia is very similar to that of 1103 Sequoia, an E[III] member discusses later. We suggest that 620 Drakonia might also belong to the E[III] subgroup.

[HERE FIGURE 8]

3.9 1103 Sequoia

We obtained a visible spectrum of 1103 Sequoia, an asteroid located in Hungaria's region with an IRAS albedo of 0.48 (Tedesco et al., 1989). The spectrum (Fig. 8) is analogous to that of 620 Drakonia: flat red sloped spectral shape from 0.45 to 0.77 μm, then a gentle drop–off of the reflectance with the presence of a shallow absorption feature (depth 1.5%) centered at $\sim$ 0.89 μm. The spectrum is similar to that presented by Bus & Binzel (2002a).

The NIR Sequoia' spectrum presented in Clark et al. (2004) shows the 0.9 and 1.8 μm absorption bands. On the basis of these data, 1103 Sequoia can be classified as an E[III] subgroup member.

3.10 1251 Hedera

1251 Hedera is located in the middle of the main belt. Its IRAS albedo is of 0.41 (Tedesco et al., 1989). We obtained a visible spectrum at the TNG telescope on Nov. 04 (Fig. 9), that clearly shows an absorption band centered at 0.9 μm. Also Clark et al. (2004) reported the presence of the 0.9 μm band, together with an absorption feature at 1.8 μm. The visible spectrum was obtained also by Fornasier & Lazzarin (2001), who reported a spectral slope value in the 5500-8000 Å range (2.58%/10^3 Å) very close to what we determine (see Table 2). 1251 Hedera might then be classify as an E[III] subgroup member.

[HERE FIGURE 9]

3.11 2048 Dwornik

2048 Dwornik is located in the Hungaria region. It has a rotational period of 3.66 hours. We observed it twice with the TNG and NTT telescope, but only in the visible range (Fig. 10). The spectrum obtained at the TNG telescope on Nov. 2004 has been cut at 0.83 μm because of large residual in the fringing corrections at longer wavelength. Its spectral slope, evaluated in the 5500-8000 Å range, is comparable to the value computed from the NTT spectrum (see Table 2). The NTT spectrum has a higher signal to noise ratio and a wider wavelength coverage. It shows an absorption band centered at

0.9 μm (3.8% depth), and a shallow feature (depth $\sim$ 1.5%) at 0.49 μm. The 0.9 μm band was detected also by Clark et al. (2004) in their NIR spectrum. The visible spectrum appears similar to the Hungaria one. We suggest that 2048 Dwornik, having both the 0.49 and 0.9 micron bands, might be an E[II] subgroup member.

[HERE FIGURE 10]

3.12 2449 Kenos

2449 Kenos is located in the Hungaria region. We obtained the first spectroscopic observations, only in the visible range, of this asteroid which has a known rotational period of 4.188 hours (Fig. 11). The spectrum is curved with a gently reddish behavior. No infrared data are available in literature for this asteroid. We do not identify any absorption features, so we suggest to classify Kenos as an E[I] subgroup member.

[HERE FIGURE 11]

3.13 2577 Litva

2577 Litva is a Hungaria family asteroid that was classify as E-type by Tholen (1989), even if its U-B and B-V colors were compatible with a TS classification. We obtain the first visible and near infrared Litva' spectrum which, as shows in Fig. 12, definitively ruled out the E-type classification. 2577 Litva has a strong absorption (band I) centered at 1.08 micron that suggests a high presence of olivine in its surface composition. The band I depth is 36%, the peak just before the olivine absorption is located at 0.78 μm, and the reflectance at 1.65 μm is 2.08. A minor content of pyroxene is present on

the asteroid surface as shown by the weaker absorption (band II) centered at 2μm. The band II / band I area ratio is 0.39±0.07 .

From our data, 2577 Litva has to be classified as an A-type asteroid. The diameter estimated from the absolute magnitude (13.18), assuming an albedo value of 0.2, is between 8-10 km. Comparing the spectral behavior of Litva with that of 9 A-type asteroids reported by Burbine & Binzel (2002), it appears that Litva has a higher abundance of olivine as compared to other small-sized A-type asteroids.

[HERE FIGURE 12]

3.14 2867 Steins

2867 Steins is the first target that will be visited by the Rosetta mission on September 2008. Its classification as an E-type asteroid was suggested based on its spectral behavior (Barucci et al. 2005), that shows a strong 0.49 μm band similar to that seen on the 64 Angelina spectrum, and on the high albedo value (0.45±0.10) determined by polarimetry (Fornasier et al., 2006). Recently Lamy et al. (2008) find a smaller albedo value of 0.34±0.06 by modelling the spectral data in the 5–38 μm wavelength range obtained with the Spitzer space telescope. This value is still consistent with the E-type classification. Moreover, Barucci et al. (2008), analyzing the Steins emissivity spectrum derived from the aforementioned Spitzer data, find that it is similar to the enstatite achondrites (aubrites) and to the enstatite mineral, confirming once again the E-type classification.

The asteroid is located at 2.36 AU, it has a rotational period is of 6.052±0.007 hours (Kuppers et al., 2007), and an estimated diameter of about 5 km.
We obtained a new spectrum on 25 May 2004 in the visible range (Fig. 13). Unfortunately, our attempt to observe the asteroid in the infrared region failed both at the TNG and NTT telescopes due to bad weather conditions or technical problems. The spectrum clearly shows the presence of the 0.49 μm band. More precisely, the band is centered at 4939±20 Å, extends from around 4300 to 5500 Å and its depth as compared to the continuum is 12%. The spectral behaviour confirms that 2867 Steins belongs to the E[II] subgroup.
We do not detect any feature in the 0.9 μm region, that is often associated to the 0.49 μm band. Barucci et al. (2005) reported the presence of a faint feature at about 0.96 μm and a flat and featureless behavior over 1 μm. The new spectrum here presented is very similar to those published by Fornasier et al. (2007), and Barucci et al. (2005), and also the spectral slope values are comparable within the errors bars. This may imply that the asteroid surface is quite homogeneous, or that we always observed the same part of the surface (the two spectra of May 04, one reported in Fornasier et al. (2007) and one here, covered almost the same portion of the surface, being separated by 3.88 rotational periods).

Steins has a deep and well–shaped 0.49 μm band, with the steepest spectral slope in the E-type population both in the 4900-5500 Å and 5500–8000 Å wavelength range (Table 2). Only the Near Earth asteroid 3103 Eger has a

similar spectral behavior (Fornasier et al., 2007), having both a high spectral slope value $S2$ and a deep ($\sim 8\%$) 0.49 μm band. On the basis of this strong spectral similarity, Fornasier et al. (2007) suggest that these two objects might have a possible common origin in spite of their presently different orbits, and that they are both remnants of an old asteroid family, the outcome of the breakup of a parent body at about 2.36 AU.

[HERE FIGURE 13]

3.15 5806 Archieroy

5806 Archieroy is located in the Hungaria region (semimajor axis of 1.96 AU) and was suggested to belong to the E-class by Gil-Hutton & Benavides (2001) on the basis of its polarimetric properties. The rotational period is of 12.16 hours. We obtain the first visible and near infrared spectrum of 5806 Archieroy at the TNG telescope during the November 2004 observing run (Fig. 14). Our data definitively ruled out the E-type classification for this asteroid. In fact, 5806 Archieroy presents two absorption bands at ~ 0.9 and 2 μm typically seen on the S-type spectra, and due to olivine and pyroxene. The first absorption band (Band I) is centered at 0.948 μm, and the second one (Band II) at 1.996 μm. The Band II/Band I area ratio is of 1.37, so 5806 Archieroy is placed in the S(V) subtype following Gaffey et al. (1993) classification scheme.

[HERE FIGURE 14]

3.16 6435 Daveross

6435 Daveross is located in the Hungarias region (semimajor axis of 1.91 AU) and was suggested to belong to the E-class by Gil-Hutton & Benavides (2001) on the basis of its polarimetric properties. We obtained the first visible spectrum of this asteroid at the TNG telescope on November 04 (Fig. 15). The spectrum is featureless, with a spectral slope $S2$ of 5.4 %/10^3 Å. No other data are available in literature. We suggest that 6435 Daveross belongs to the E[I] subtype

3.17 6911 Nancygreen

6911 Nancygreen is another asteroid located in the Hungaria region (semimajor axis of 1.93 AU) that was suggested to belong to the E-class by Gil-Hutton & Benavides (2001) on the basis of its polarimetric properties. Its rotational period is of 5.38 hours. We observed this asteroid at the NTT telescope on Jan. 07, in the visible range. The spectrum shows a faint band centered at 4966±0.30 Å, about 3% depth as compared to the continuum (Fig. 15). There are no other data in the literature about this asteroid. On the basis of the visible spectrum, we suggest that 6911 Nancygreen belongs to the E[II] subgroup.

[HERE FIGURE 15]

3.18 7579 1990 TN1

1990 TN1 is a Hungaria family asteroid that, on the basis of its polarimetric properties, was suggested to belong to the E-type by Gil-Hutton & Benaviez

(2001). We obtained the first visible and near infrared spectrum of 1990 TN1 (Fig. 16) that ruled out the E-type classification. The spectrum shows a sharp absorption band centered at 1.04 micron with a depth of 39% as respect to a continuum line, indicative of the presence of olivine. The relative reflectance value at 1.65 micron is 2.01, and there is no evidence of the pyroxene absorption band at 2 micron. 1990 TN1 is then a typical olivine rich A-type asteroid.

[HERE FIGURE 16]

4 Spectral modelling

E–type asteroids are thought to be the parent bodies of the aubrite meteorites (Burbine et al., 2002a). These meteorites are composed primarily of enstatite, a Ca–rich silicate; metal Fe is also present in minor amounts, according to the theory that enstatitic meteorites formed in an O–poor environment. Other minerals, also supposed to be present on the aubrites, are feldspates (1-16%), diopside (0.2-8%), olivine (0.3-10%), Fe-Ni rich minerals (0.1-3.7%), and troilite (0.1-7%) (Reid & Cohen, 1967; Olsen et al., 1977; Watters & Prinz, 1979; Watters et al., 1980; Keil et al., 1989), and, in minor amount, oldhamite, caswellsilverite, daubreelite, alabandite and shreibersite (Keil & Fredrikson, 1963; Okada & Keil, 1982).

In order to investigate the possible surface composition of the E-type asteroids, we attempt to reproduce their spectral behaviors by obtaining synthetic spectra of different geographical mixtures (spatially segregated) of meteorites and minerals (Fornasier et al., 2004b; Dotto et al., 2006). We

considered meteorites and minerals that are compositionally related to the igneous asteroids, such as aubrite achondrites, enstatite, orthopyroxene, diopside, troilite and oldhamite. We limited our investigation to the E-type asteroids for which we have both the visible and near infrared data. We made the assumption that our combined visible and near infrared spectra, acquired on two different nights and not simultaneously, are representative of the same reflecting surface. Our first aim was to identify the meteorites samples with a spectral behavior very similar to that of the observed asteroids; should that not be the case, we enriched the meteorites with some minerals, already known to be constituent of the aubrites, in order to reproduce both the asteroid's spectral behavior and its albedo value. We took into account the complete sample of minerals and meteorites included in the RELAB catalog. We developed a Fortran code to calculate the reflectance of the mixtures which better match the observed asteroids spectra, according to a Chi–Square test. We decided to consider only the mixtures composed of no more than 3 endmembers, as, including a greater number of compounds, the fit improves but it becomes very difficult to control the relationship between the asteroids composition and meteorites/minerals abundances. The main meteorites and minerals samples used in our models are listed in Table 3 and represented in Fig. 17.

[HERE FIGURE 17 and 18]

For asteroid *44 Nysa* it was not possible to find a compositional model able to reproduce both the visible and near-infrared spectral behavior, and the albedo value. The spectral trend of the near-infrared part of the spectrum

is well reproduced by mixing the meteorite Peña Blanca (55%) with a huge amount of troilite (45%). This mixture, nevertheless, has a visible spectrum steeper compared to that of Nysa (Fig. 18, continuous line) and a lower albedo (0.33). In addition, is not easy to justify such huge amount of troilite, as it is present in lower percentages (<10%) inside the aubrites. A second possible model of the surface composition of Nysa is given by a mixture made of the aubrite meteorite Peña Blanca (77%), enriched with troilite (8%) and diopside (15%); the albedo value of the mixture is 0.49, in good agreement with the asteroid one (Fig. 18, dashed line), although the spectral slope is not well reproduced.

Asteroid *64 Angelina* (IRAS albedo=0.43) is compatible with the aubrite ALH78113 (albedo = 0.49). To better reproduce the asteroid spectral behavior, we enriched the meteorites with oldhamide (Fig. 18). The model we propose is then constituted of 92% of meteorite ALH78113 and 8% of oldhamite, and has an albedo value of 0.47.

For asteroid *214 Aschera* we propose a mixture (Fig. 18) constituted of 88% of the aubrite Peña Blanca enriched with a 12% of orthopyroxene. This simple mixture reproduces quite well the visible and near infrared behaviour, and in particular the 0.9 μm absorption band. The albedo of the mixture is 0.53, higher than the asteroid value (0.40).

Asteroid *317 Roxane*, as previously discussed, shows both the 0.9 and 1.8 μm absorption features. We find a good spectral match between the asteroid spectrum and that of the aubrite Peña Blanca (Fig. 18). Moreover, also the meteorite albedo value (0.52) is very close to the asteroid one (0.49). This

is the first meteorite– E[III] asteroid match found to date (Gaffey & Kelley, 2004).

For *437 Rhodia*, it is again not easy to reproduce the well pronounced 0.9 μm band, the overall spectral behavior and the very high albedo value (0.70±0.08 in Tedesco et al., 2002, but 0.56±0.03 in Tedesco et al., 1989). A mixture of the aubrite meteorite Peña Blanca (90%) with 10% of orthopyroxene gives a high albedo value (0.53) and nicely reproduced the 0.9 μm absorption band and the spectral behaviour in the visible range, but does not match the infrared data (Fig. 18, dash line). Another model is proposed, constituted of 85% of the aubrite Y-793592 and 15% orthopyroxene, for an albedo value of 0.47 (Fig. 18, continuous line). This mixture better reproduces the spectral behaviour of Rhodia in the infrared range, but does not match the visible data.

For *2867 Steins* we considered the visible spectrum presented here together with the near infrared one published by Barucci et al. (2005). The resulting spectrum is quite red and presents a wide band at about 0.5 μm. The best model we find is constituted of 65% of the meteorite ALH78113 and 35% of oldhamite. The model albedo is 0.38, in good agreement with the albedo of Steins (0.34±0.06) derived from radiometric analysis of the IRS - Spitzer data (Barucci et al., 2008), and inside the error bars of the polarimetric albedo (0.45±0.10, Fornasier et al., 2006). Our model is in good agreement with one of the models recently published by Nedelcu et al. (2007) given by a geographycal mixture of enstatite (57%), oldhamite (42%) and orthopyroxene (1%). At the present time, oldhamite is the only endmember

that, added to the ALH78113 meteorite, allow us to fit both the deep 0.5 μm band and the visible red slope of Steins. All the other attempts made with more than 2 endmembers failed to satisfactory fit the Steins spectral behavior, and in any case a relevant percentage ($> 18\%$) of oldhamite was needed to reproduce the 0.5 μm feature.

Such a huge amount of oldhamite on the Steins' surface is quite surprising, due to the fact that the percentage of sulfide oldhamite found in aubrite samples is smaller than 1% (Burbine et al., 2002b). Nevertheless, it is well known that oldhamite is extremely unstable in terrestrial conditions, and we cannot exclude that the abundance of oldhamite in aubrite materials and/or on the surface of the aubrite parent bodies might actually be larger than the one detected in terrestrial laboratory (Clark et al. 2004; Burbine et al., 2002b).

5 Discussion

[HERE FIGURE 19]

Considering our observations and those available in literature, the known E-type population can be divided as follow:

5 E[I] members (504, 1025, 2449, 6435, and 144898);

8 E[II] members (64, 434, 2048, 2035, 2867, 3103, 4660, and 6911), but the faint absorption bands on 2048 and 6911 need to be confirmed by independent observations;

8 E[III] members (44, 214, 317, 437, 620, 1103, 1251, and 3050), but the faint absorption band at 0.9 μm on 620 Drakonia needs to be confirmed.

Looking into the list of the known or suggested E-type asteroids presented by Clark et al. (2004), 3 of the listed asteroids (2577, 5806 and 7579) have spectral behaviors different from the E-type objects and should not be considered E-class members. On the other side, 437 Rhodia, 2867 Steins, and 144898 2004 VD17 have high albedo values and spectra consistent with the E-type classification and should be added to the list (Barucci et al., 2005; Fornasier et al., 2006; De Luise et al., 2007). Also 3050 Carrera, on the basis of its spectral behavior (but the albedo is not known) probably belongs to the E-type (Barucci et al., 2005).

In Fig. 19 we plot the spectral slope value $S2$ evaluated in the 5500–8000 Å wavelength range versus the semimajor axis and inclination for the E-type members investigated in this paper and those whose spectra are available in literature. The three different sub-group members are represented with different symbols: E[I] in triangles, E[II] in circles, and E[III] in squares. The points are expanded with size proportional to the diameter of each target (see Table 2). The E[III] members are situated mostly between 2.2 and 2.7 AU, with only 1 member populating the Hungaria region. They have the lower mean $S2$ spectral slope value (2.43±1.12) and all, except 1103 Sequoia, have inclinations lower than 8 degrees. The E[I] members have a mean S3 slope of 4.59±1.32; 3 are located in the Hungaria family, one is a NEO and the biggest member has the largest semimajor axis (2.72 AU) inside the E-type class. The E[II] members have the largest mean $S2$ slope value (5.44±1.45). Four members populated the Hungaria regions, 2 are NEOs, and 2 are main

belt members (2867 Steins, the Rosetta target, and 64 Angelina, the largest member). The spectral similarity of 2867 Steins and the NEO 3103 Eger was reported in Fornasier et al. (2007), who explore the possibility that the two objects are both remnants of an old asteroid family, the outcome of the breakup of a parent body at about 2.36 AU. Despite their presently different orbits, numerical orbital integrations show that there is a dynamical pathway between the present orbit of Steins, possibly the largest remnant of the family, and Earth–crossing orbits like that of Eger. Members of the putative Steins family might be driven by the Yarkovsky force and gravitational influence of the planets into the 3:1 and 7:2 mean motion resonances with Jupiter and finally be injected in the Earth–crossing region.

6 Summary

We present the results of a survey on igneous E-type asteroids started on 2004 at the TNG and NTT telescopes. We got new visible spectra of 18 asteroids, and 8 of them were observed also in the near infrared range. We confirm that the small E-type population shows 3 different mineralogies and we classified the observed objects in the 3 subgroups following Gaffey & Kelley (2004) classification scheme.

Few objects (i.e. 64 Angelina, 317 Roxane, and 434 Hungaria) present different spectral behaviors in our data and those coming from literature, and we suggest that they may have an inhomogeneous surface composition. For these asteroids, additional observation covering the whole rotational period are needed to fully investigate their surface composition.

We investigated the spectral slope distribution for the three E-subgroups members versus the asteroids' semimajor axis and inclination. We also include in our sample the spectra of 6 E-type available in literature and not observed in this work, for a total sample of 21 E-type asteroids.

E[III] subgroup members have the lowest mean spectral slope value inside the whole sample. Within the E-type population, they are the more distant from the Sun, being located mainly between 2.2-2.7 AU in low inclination orbit. E[II] members has the highest spectral slope inside the sample. Both E[II] and E[I] members are mainly located in the Hungaria region, but some members are present both in the NEA population and in the main belt.

Finally, for the five E-type asteroids observed both in the visible and near infrared range, plus 2867 Steins, a target of the Rosetta mission, we attempt to model their surface composition using geographycal mixtures of aubrite meteorites and minerals. The spectrum of the E[III]-type asteroid 317 Roxane is nicely matched by the aubrite Peña Blanca, that has also a similar high albedo value. We then suggest that this aubrite might have 317 Roxane as a possible parent body. The compositional model that better fit the E[III] type 214 Aschera is mainly composed of aubrite Peña Blanca enriched with orthopyroxene. Also the spectrum and albedo of the E[II]-type 64 Angelina and 2867 Steins might be reproduced by an aubrite, ALH78113 , but it must be enriched with a considerably amount of oldhamite. On the other hand, the compositional models proposed for the E[III]-type asteroids 44 Nysa and 437 Rhodia do not match their whole spectral behavior and albedo values.

The results of the spectral modelling show that two different aubrites match

the albedo and the V+NIR spectral behavior of two different E-type asteroids. The aubrite Peña Blanca nicely matches the spectrum and albedo of 317 Roxane, that could be its parent body, and, enriched with orthopyroxene, that of 214 Aschera, so it is related to the E[III] subgroup asteroids. The aubrite ALH78113, the only one surveyed to now showing the $\sim$ 0.5 μm band, is clearly related to the E[II] subgroup, but it must be enriched in oldhamite to give rise to the strong 0.5 μm band seen in the Angelina and Steins spectra.

Acknowledgemt

The authors thank F. DeMeo for her help in the language revision. This research utilizes spectra acquired with the NASA RELAB facility at Brown University by: McCoy & Burbine; Cloutis; Hiroi; Hiroi, Zolensky & Lipschults; McFadden; Pieters & Britt; Pieters & Crown; Pieters & Sunshine. This work has been partly supported by an Europlanet personnel exchange grant.

References

Barucci, M. A., Fulchignoni, M., Fornasier, S., Dotto, E., Vernazza, P., Birlan, M., Binzel, R. P., Carvano, J., Merlin, F., Barbieri, C., Belskaya, I., 2005. Asteroid target selection for the new Rosetta mission baseline. 21 Lutetia and 2867 Steins. Astron. Astroph. 430, 313–317.

Barucci, M. A., Fornasier, S., Dotto, E., Lamy, P., Jorda, L., Groussin, O., Brucato, J.R., Carvano, J., Alvarez-Candal, A., Cruikshank, D., Fulchignoni, M., 2008. Asteroids 2867 Steins and 21 Lutetia: surface composition from far infrared observations with the Spitzer space telescope. Astron. Astroph. 477, 665-670

Bus, S. J., Binzel, R. P., 2002a. Phase II of the Small Main-Belt Asteroid Spectroscopic SurveyThe Observations. Icarus 158, 106-145.

Bus, S. J., Binzel, R. P., 2002b. Phase II of the Small Main-Belt Asteroid Spectroscopic SurveyA Feature-Based Taxonomy. Icarus 158, 146-177.

Binzel, R. P., Birlan, M. Bus, S. J., Harris, A. W., Rivkin, A. S., Fornasier, S. 2004. Spectral observations for near-Earth objects including potential target 4660 Nereus : Results from Meudon remote observations at the NASA Infrared Telescope Facility (IRTF). Planetary and Space Science 52, 291-296.

Binns, R.A., (1969), A Chondritic Inclusion of Unique Type in the Cumberland Falls Meteorite, Meteorite Research, D. Reidel Publ. Co., Hingham, Mass., 696-704.

Burbine, T. H., Cloutis, E. A., Bus, S. J., Meibom, A., Binzel, R. P., 1998. The detection of troilite (FeS) on the surfaces of E-class asteroids. Bull. Am. Astron. Soc. 30, 711.

Burbine, T.H., McCoy, T.J., Meibom, A., 2002a. Meteorite parent bodies, in Asteroids III, Bottke, W. et al. Editors, Univ. of Arizona Press, Tucson.

Burbine, T. H., McCoy, T. J., Nittler, L., Benedix, G., Cloutis, E., Dickenson, T. 2002b. Spectra of extremely reduced assemblages: Implications for

Mercury. Meteorit. Planet. Sci. 37, 12331244.

Burbine, T.H. & Binzel, R. P., 2002. Small Main Belt Asteroid Spectroscopic Survey in the Near Infrared. Icarus 159, 468–499 ‘

Busarev, V. V., 1998. Spectral Features of M-Asteroids: 75 Eurydike and 201 Penelope. Icarus 131, 32-40.

Busarev, V. V., 2002. Hydrated Silicates on M-, S-, and E-Type Asteroids as Possible Traces of Collisions with Bodies from the Jupiter Growth Zone. Solar System Res. 36, 35-42

Clark, B.E., Bus, S.J., Rivkin, A.S., McConnochie, T., Sander, J., Shah, S., Hiroi, T., Shepard, M., (2004), E-Type asteroid spectroscopy and compositional modeling, JGR 109, E02001, doi:10.1029/2003JE002200.

Delbó M., Harris, A.W., Binzel, R.P., Pravec P., Davies, J. K., 2003. Keck observations of near-Earth asteroids in the thermal infrared. Icarus 166, 116130.

De Luise, F., Perna, D., Dotto, E., Fornasier, S., Belskaya, I., Boattini, A., Valsecchi, G. B., Milani, A., Rossi, A., Lazzarin, M., Paolicchi, P., Flchignoni, M., 2007. Physical investigation of the potentially hazardous asteroid (144898) 2004 VD17. Icarus 191, 628-635

Dotto, E., Fornasier, S., Barucci, M. A., Licandro, J., Boehnhardt, H., Hainaut, O., Marzari, F., de Bergh, C., de Luise, F., 2006. The surface composition of Jupiter Trojans: Visible and near-infrared survey of dynamical families. Icarus 183, 420-434

Fornasier, S., & Lazzarin, M., 2001. E-Type asteroids: Spectroscopic investigation on the 0.5μm absorption band. Icarus 152, 127-133.

Fornasier, S., Dotto, E., Marzari, F., Barucci, M.A., Boehnhardt, H., Hainaut, O., de Bergh, C., 2004a. Visible spectroscopic and photometric survey of L5 Trojans : investigation of dynamical families. Icarus 172, 221–232.

Fornasier, S., Dotto, E., Barucci, M. A., Barbieri, C., 2004b. Water ice on the surface of the large TNO 2004 DW. Astron. Astroph. 422, L43-L46.

Fornasier, S., Belskaya, I., Fulchignoni, M., Barucci, M. A., Barbieri, C., (2006), First albedo determination of 2867 Steins, target of the Rosetta mission. Astron. Astroph. 449, L9-L12.

Fornasier, S., Marzari, F., Dotto, E., Barucci, M. A., Migliorini, A., 2007. Are the E-type asteroids (2867) Steins, a target of the Rosetta mission, and NEA (3103) Eger remnants of an old asteroid family? Astron. Astroph. 474, 29–32

Gaffey, M. J., J. F. Bell, and D. P. Cruikshank 1989. Reflectance spectroscopy and asteroids surface mineralogy. In *Asteroids II* (R.P. Binzel, T. Gehrels, and M. S. Matthews, Eds.), pp. 98-127. Univ. of Arizona Press, Tucson.

Gaffey, M. J., K. L. Reed, and M. S. Kelley 1992. Relationship of E-type Apollo asteroids 3103 (1982 BB) to the enstatite achondrite meteorites and Hungaria asteroids. Icarus 100, 95-109.

Gaffey, M. J., Burbine, T. H., Piatek, J. L., Reed, K. L., Chaky, D. A., Bell, J. F., Brown, R. H., 1993. Mineralogical variations within the S-type asteroids class. Icarus 106, 573-602

Gaffey, M. J. & Kelley, M.S., (2004), Mineralogical variation among high

albedo E-type asteroids: implications for asteroid igneous processes, Lunar and Plan. Sci. Conference, abstract no. 1812

Gil-Hutton, R. & Benavidez, P., 2001. Polarimetric albedo of Hungarian asteroids: Preliminary results. Paper presented at the International Conference Asteroids 2001, Osserv. Astron. di Palermo, Palermo, Italy, 11-16 June.

Harris, A. W., Mueller, M., Delb, M. Bus, S. J., 2007. Physical characterization of the potentially hazardous high-albedo Asteroid (33342) 1998 WT24 from thermal-infrared. Icarus 188, 414-424.

Keil, K. & Fredriksson, K., (1963), Electron microprobe analysis of some rare minerals in the Norton County achondrite. Geochim. Cosmochim. 27, 939-942.

Keil, K., Ntaflos, Th., Taylor, G.J., Brearley, A.J., Newsom, H.E., (1989), The Shallowater aubrite - Evidence for origin by planetesimal impacts. Geochim. Cosmochim. 53, 3291-3307.

Kelley, M. S. & Gaffey, M. J., 2002. High-albedo asteroid 434 Hungaria: Spectrum, composition and genetic connections. Meteor. & Plan. Science 37, 1815–1827

King, T. V. V., & R. N. Clark 1989. Spectral characteristics of chlorites and Mg-serpentines using high resolution reflectance spectroscopy. J. Geophys. Res. 94, 13997-14008.

Kuppers, M., Mottola, S., Lowry, S. C., A'Hearn, M. F., Barbieri, C., Barucci, M. A., Fornasier, S., Groussin, O., Gutirrez, P., Hviid, S. F., Keller, H. U., Lamy, P., 2007. Determination of the light curve of the Rosetta target

asteroid (2867) Steins by the OSIRIS cameras onboard Rosetta. Astron. Astroph. 462, 13–16

Lamy, P., Jorda, L., Fornasier, S., Groussin, O., Barucci, M.A., Carvano, J., Dotto, E., Fulchignoni, M., Toth, I., 2008. Asteroid Steins: III. Spitzer space telescope observations, size determination and thermal properties. Astron. Astroph., submitted

McCoy, T.J., Dickinson, T. L., Lofgren, G. E., 1999. Partial melting of the Indarch (EH4) Meteorite: A textural, chemical and phase relations view of melting and melt migration. Meteor. & Plan. Science 34, 735-746

Nedelcu, D. A., Birlan, M., Vernazza, P., Binzel, R. P., Fulchignoni, M., Barucci, M. A., 2007. E-type asteroid (2867) Steins: flyby target for Rosetta. Astron. Astroph. 473, 33-36

Okada, A. & Keil K., 1982. Caswellsilverite, NaCrS2: a new mineral in the Norton County enstatite achondrite. Amer. Mineral. 67, 132–136.

Kelley M. S. & Gaffey M. J., 2002. High albedo asteroid 434 Hungaria: spectrum, composition and genetic connections. Meteoritics & Plan. Science 37, 1815-1827.

Olsen, E.J., Bunch, T.E., Jarosewich, E., Noonan, A.F., Huss, G.I., 1977. Happy Canyon - A new type of enstatite achondrite. Meteoritics 12, 109–123.

Reid, A.M. & Cohen, A.J., (1967), Some characteristics of enstatite from enstatite achondrites. Geochim. Cosmochim. 31, 661–670.

Rivkin, A. S., E. S. Howell, D. T. Britt, L. A. Lebofsky, M. C. Nolan, and D. D. Branston 1995. 3-μm spectrophotometric survey of M and E class asteroids. Icarus 117, 90-100.

Sawyer, S. R., 1991. A high resolution CCD spectroscopic survey of low albedo main belt asteroids. Ph.D. thesis, University of Texas, Austin, Texas, USA.

Tedesco, J.G., Williams, D.L., Matson, J.C., Gradie, Lebofsky, L.A., 1989. Three-parameter asteroid taxonomic classifications. In *Asteroids II* (R.P. Binzel, T. Gehrels, and M. S. Matthews, Eds.), pp. 1151-1161. Univ. of Arizona Press, Tucson.

Tedesco, J.G., Noah, P. V., Noah, M., Price, S. D., 2002. The Supplemental IRAS Minor Planet Survey. Astron. Journal 123, 1056-1085.

Tholen, D. J. 1989. Asteroids taxonomy. In *Asteroids II* (R.P. Binzel, T. Gehrels, and M. S. Matthews, Eds.), pp. 1139-1153. Univ. of Arizona Press, Tucson.

Veeder, G. J., Hanner, M. S., Matson, D. L., Tedesco, E. F., Lebofsky, L. A., Tokunaga, A. T., 1989. Radiometry of near-earth asteroids. Astron. Journal 97, 1211-1219.

Vilas, F., E. C. Hatch, S. M. Larson, S. R. Sawyer, and M. J. Gaffey 1993. Ferric iron in primitive asteroids: a 0.43 μm absorption feature. Icarus 102, 225-231.

Watters, T.P., & Prinz, M., (1979), Aubrites: Their origin and relationship to enstatite chondrites, Proc. Lunar Planet. Sci. Conf., 10th, 1073-1093.

Watters, T.P., Prinz, M., Rambaldi, E.R., Wasson, J.T., 1980. ALHA 78113, Mt. Egerton and the Aubrite Parent Body. Meteoritics 15, 386.

Zellner, B., M. Leake, J. G. Williams, Morrison, D., 1977. The E asteroids and the origin of the enstatite achondrites. Geochim. Cosmochim. Acta 41,

1759-1767.

Tables

Table 1: Observational circumstances.

Object	Night	UT-start (hh:mm)	T_{exp} (s)	Tel.	Instr.	Grism	airm.	Solar Analog (airm.)
44 Nysa	29 Feb. 04	06:58	40	TNG	DOLORES	LR-R	1.40	la107684 (1.15)
44 Nysa	13 Aug. 05	05:40	30	NTT	EMMI	GR1	1.05	HD1835 (1.07)
44 Nysa	12 Aug. 05	05:59	60	NTT	SOFI	GBF	1.06	hip103572 (1.06)
44 Nysa	12 Aug. 05	06:01	60	NTT	SOFI	GRF	1.06	hip103572 (1.06)
44 Nysa	20 Jan. 07	04:13	5	NTT	EMMI	GR1	1.65	la98-978 (1.35)
64 Angelina	16 Nov. 04	00:49	50	TNG	DOLORES	LR-R	1.02	hyades64 (1.03)
64 Angelina	16 Nov. 04	00:52	80	TNG	DOLORES	MR-B	1.02	hyades64 (1.03)
64 Angelina	19 Nov. 04	01:33	120	TNG	NICS	AMICI	1.08	Hyades64 (1.01)
214 Aschera	25 May 04	10:18	150	NTT	EMMI	GR1	1.11	la112-1333 (1.17)
214 Aschera	18 Nov. 04	19:49	240	TNG	NICS	AMICI	1.24	la93-101 (1.34)
317 Roxane	29 Feb. 04	03:04	120	TNG	DOLORES	LR-R	1.14	hd89010 (1.02)
317 Roxane	29 Feb. 04	03:07	180	TNG	DOLORES	LR-B	1.14	hd89010 (1.18)
317 Roxane	13 Aug. 05	02:22	180	NTT	EMMI	GR1	1.07	HD1835 (1.07)
317 Roxane	13 Aug. 05	05:21	180	NTT	EMMI	GR1	1.10	HD1835 (1.07)
317 Roxane	12 Aug. 05	05:16	320	NTT	SOFI	GBF	1.09	hip096165 (1.09)
317 Roxane	12 Aug. 05	05:24	320	NTT	SOFI	GRF	1.10	hip096165 (1.09)
317 Roxane	20 Jan. 07	03:24	180	NTT	EMMI	GR1	1.57	Hyades64 (1.45)
434 Hungaria	16 Nov. 04	00:10	180	TNG	DOLORES	LR-R	1.51	hyades64 (1.03)
434 Hungaria	16 Nov. 04	00:15	180	TNG	DOLORES	MR-B	1.50	hyades64 (1.03)
437 Rhodia	29 Feb. 04	02:42	180	TNG	DOLORES	LR-R	1.28	la107684 (1.20)
437 Rhodia	29 Feb. 04	02:48	180	TNG	DOLORES	LR-B	1.28	la107684 (1.20)
437 Rhodia	01 Mar. 04	04:17	480	TNG	NICS	AMICI	1.54	la102-1081 (1.46)
504 Cora	29 Feb. 04	05:55	180	TNG	DOLORES	LR-R	1.28	la107684 (1.20)
504 Cora	29 Feb. 04	05:59	180	TNG	DOLORES	LR-B	1.29	la107684 (1.20)
504 Cora	13 Aug. 05	00:16	300	NTT	EMMI	GR1	1.02	HD144585 (1.05)
620 Drakonia	20 Jan. 07	08:06	1800	NTT	EMMI	GR1	1.19	la98-978 (1.22)
1103 Sequoia	20 Jan. 07	01:01	600	NTT	EMMI	GR1	1.64	Hyades64 (1.45)
1251 Hedera	18 Nov. 04	06:01	600	TNG	DOLORES	LR-R	1.06	hyades64 (1.40)
1251 Hedera	18 Nov. 04	06:13	720	TNG	DOLORES	MR-B	1.07	hyades64 (1.40)
2048 Dwornik	16 Nov. 04	05:42	1200	TNG	DOLORES	LR-R	1.26	hyades64 (1.03)
2048 Dwornik	20 Jan. 07	01:17	2400	NTT	EMMI	GR1	1.54	Hyades64 (1.45)
2449 Kenos	20 Jan. 07	06:06	2400	NTT	EMMI	GR1	1.16	la98-978 (1.22)
2577 Litva	29 Feb. 04	05:26	480	TNG	DOLORES	LR-R	1.29	la107684 (1.20)
2577 Litva	29 Feb. 04	05:35	360	TNG	DOLORES	LR-B	1.30	la107684 (1.20)
2577 Litva	01 Mar. 04	05:44	720	TNG	NICS	AMICI	1.32	la107648 (1.20)
2867 Steins	25 May 04	00:16	1200	NTT	EMMI	GR1	1.45	la102-1081 (1.22))
5806 Archieroy	16 Nov. 04	02:02	480	TNG	DOLORES	LR-R	1.13	HD28099 (1.05)
5806 Archieroy	19 Nov. 04	02:20	1440	TNG	NICS	AMICI	1.13	la98-978 (1.17)
6435 Daveross	16 Nov. 04	03:33	900	TNG	DOLORES	LR-R	1.60	hyades64 (1.03)
6911 Nancygreen	20 Jan. 07	07:17	1200	NTT	EMMI	GR1	1.06	la102-1081 (1.14)
7579 1990TN1	15 Nov. 04	22:58	600	TNG	DOLORES	LR-R	1.03	hyades64 (1.03)
7579 1990TN1	19 Nov. 04	00:47	1080	TNG	NICS	AMICI	1.30	la93-101 (1.34)

Table 2: Spectral slopes for different wavelength range for the investigated asteroids. $S1$, $S2$, and $S3$ are the spectral slopes evaluated respectively in the 4900-5500 Å, 5500-8000 Å, and 8000-9000 Å wavelength range. [a]: visible spectrum taken from Bus & Binzel (2002a); [b]: visible spectrum and albedo taken from Fornasier & Lazzarin (2001); [c]: visible spectra taken from Fornasier et al. (2007); [d]: visible spectrum taken from Barucci et al. (2005); [e]: visible spectrum taken from Binzel et al. (2004) and the albedo from Delbo et al. (2003); [f]: visible spectrum and albedo taken from De Luise et al., (2007). Diameter, albedo, and rotational periods are taken from IRAS observations (Tedesco et al. 1989; 2002) and from the Asteroid physical parameters data in the Jet Propulsional Laboratory Horizon webpage (http://ssd.jpl.nasa.gov/horizons.cgi#top). Diameters marked with * are evaluated from the asteroid absolute magnitude assuming an albedo value of 0.4. Tx is the suggested taxonomy.

asteroid	a (AU)	e	i (^{o})	D (Km)	albedo	rot. (h)	$S1$ (%/10^3 Å)	$S2$ (%/10^3 Å)	$S3$ (%/10^3 Å)	Tx
44 Nysa (Jan07)	2.42	0.148	3.70	70.6	0.55	6.42	5.92±0.89	1.52±0.61	-3.83±0.69	E[III]
44 Nysa (Feb 04)	2.42	0.148	3.70	70.6	0.55	6.42	–	3.18±1.02	-1.47±0.73	
44 Nysa (Aug 05)	2.42	0.148	3.70	70.6	0.55	6.42	5.39±0.80	2.34±0.61	-1.31±0.63	
64 Angelina	2.68	0.124	1.30	59.8	0.43	8.75	16.32±0.84	4.06±0.61	1.62±0.65	E[II]
214 Aschera	2.61	0.029	3.43	23.2	0.52	6.83	6.03±1.16	1.15±0.62	-4.02±0.81	E[III]
317 Roxane (Aug05A)	2.28	0.085	1.76	18.7	0.49	8.16	4.38±1.18	2.65±0.62	-4.18±0.89	E[III]
317 Roxane (Aug05B)	2.28	0.085	1.76	18.7	0.49	8.16	6.16±0.97	2.72±0.61	-1.26±0.69	
317 Roxane (Jan 07)	2.28	0.085	1.76	18.7	0.49	8.16	9.40±0.88	2.92±0.61	-0.61±0.65	
317 Roxane (Feb 04)	2.28	0.085	1.76	18.7	0.49	8.16	10.73±1.10	4.43±0.61	–	
434 Hungaria	1.94	0.073	22.50	10.0	0.46	26.51	14.49±0.85	6.09±0.61	3.65±0.73	E[II]
437 Rhodia	2.38	0.247	7.35	13.2	0.70	–	11.24±1.09	2.90±0.62	-9.48±0.86	E[III]
504 Cora	2.72	0.217	12.89	30.0	0.34	24.06	10.93±0.81	5.43±0.62	2.83±0.84	E[I]
504 Cora	2.72	0.217	12.89	30.0	0.34	24.06	3.92±2.44	4.42±0.65	1.75±1.34	
620 Drakonia	2.43	0.134	7.73	11.6*	–	5.485	7.49±0.95	3.66±0.61	-0.44±0.69	E[III] ?
1025 Riema[a]	1.98	0.039	26.8	7.0	–	3.58	20.23±2.59	5.63±0.61	-2.37±0.74	E[I]
1103 Sequoia	1.93	0.094	17.90	6.1	0.48	3.049	7.55±0.92	3.27±0.61	-0.14±0.71	E[III]
1251 Hedera	2.71	0.154	6.03	14.6	0.41	15.01	3.97±0.86	2.86±0.62	-3.23±1.90	E[III]
2035 Stearns[b]	1.88	0.131	27.7	5.5	–	85.0	12.50±0.56	3.98±0.62	-3.81±1.18	E[II]
2048 Dwornik (Nov 04)	1.95	0.042	23.74	5.0*	–	3.66	15.54±1.21	4.51±0.63	-1.39±0.84	E[II]
2048 Dwornik (Jan 07)	1.95	0.042	23.74	11.6*	–	3.66	–	5.96±1.02	–	
2449 Kenos	1.91	0.168	24.98	3.0*	–	4.19	13.73±1.26	5.16±0.63	2.30±0.86	E[I]
2577 Litva	1.90	0.138	22.90	–	–	2.82	18.21±1.31	12.83±0.62	-4.56±0.84	A
2867 Steins	2.36	0.145	9.94	4.6	0.45	6.05	34.03±1.49	8.10±0.65	2.89±1.03	E[II]
2867 Steins (May 04)[c]	2.36	0.145	9.94	4.6	0.45	6.05	32.02±1.59	6.93±0.65	2.24±1.03	
2867 Steins (Aug 05)[c]	2.36	0.145	9.94	4.6	0.45	6.05	33.05±1.35	7.62±0.64	2.45±0.86	
3050 Carrera[d]	2.22	0.188	1.306	3.6	–	–	7.82±1.96	0.50±0.65	-8.30±1.3	E[III]
3103 Eger[c]	1.40	0.354	20.93	1.4	0.63	5.70	24.90±1.28	7.43±0.63	3.99±0.76	E[II]
4660 Nereus[e]	1.49	0.360	1.432	1.0	0.55	15.10	5.68±2.06	4.32±0.55	2.53±1.63	E[II]
5806 Archieroy	1.96	0.36	20.82	–	–	12.16	–	9.50±0.63	-8.13±0.96	S[V]
6435 Daveross	1.91	0.057	23.43	3.0*	–	–	–	5.37±0.64	2.40±1.27	E[I]
6911 Nancygreen	1.93	0.090	22.90	4.9*	–	5.38	12.30±1.30	4.76±0.65	-0.26±0.95	E[II]
7579 1990 TN1	1.98	0.065	16.98	–	–	–	–	10.71±0.67	-8.11±0.98	A
144898 2004 VD17[f]	1.51	0.588	4.22	0.64	0.45	1.99	7.76±2.74	2.38±0.70	–	E[I]

Name	**RELAB code**	**Grain size μm**
Meteorites		
Abee	c1mt40	<125
Bishopville	c1tb47	<125
Happy Canyon	cbea03	<45
Mayo Belwa	s1tb46	<125
Norton Country	cbea04	<45
Peña Blanca	c1tb45	<125
ALH 78113	c4lm04	Frag.
Y-793592	BKR1MP105	<125
Minerals		
clinopyroxene	c1pp21	<45
orthopyroxene	c1pe30	<45
diopside	c2pd01	<45
forsterite	c1po76	<45
oldhamide	c1tb38	<125
troilite	cdmb06	63 – 125

Table 3: *List of the main meteorites and minerals used in our models, selected from RELAB catalogue.*

Figure captions

Fig. 1 - Visible and near infrared spectra of 44 Nysa.

Fig. 2 - Visible and near infrared spectrum of 64 Angelina.

Fig. 3 - Visible and near infrared spectrum of 214 Aschera.

Fig. 4 - Visible and near infrared spectra of 317 Roxane.

Fig. 5 - Visible spectrum of 434 Hungaria.

Fig. 6 - Visible and near infrared spectra of 437 Rhodia.

Fig. 7 - Visible spectra of 504 Cora.

Fig. 8 - Visible spectra of 620 Drakonia and 1103 Sequoia.

Fig. 9 - Visible spectrum of 1251 Hedera.

Fig. 10 - Visible spectrum of 2048 Dwornik.

Fig. 11 - Visible spectrum of 2449 Kenos.

Fig. 12 - Visible and near infrared spectra of 2577 Litva.

Fig. 13 - Visible spectrum of 2867 Steins, a target of the Rosetta mission.

Fig. 14 - Visible and near infrared spectrum of 5806 Archieroy.

Fig. 15 - Visible spectra of 6435 Daveross and 6911 Nancygreen.

Fig. 16 - Visible and near infrared spectrum of 7579 1990 TN1.

Fig. 17 - Spectra of the main endmembers (meteorites and minerals) used in our compositional models of E-type asteroids

Fig. 18 - Compositional mixtures (represented as continuous line) proposed for the asteroids with visible and near-infrared spectra. In the case of 317 Roxane, the spectrum of the aubrite Peña Blanca nicely fit the asteroid's spectral behavior.

Fig. 19 - Spectral slope value ($S3$) versus the semimajor axis (left) and the orbital inclination (right). E[I] subgroup members are displayed with triangles, E[II] with circles, E[III] with squares. The size is proportional to the asteroids' diameter.

Figures

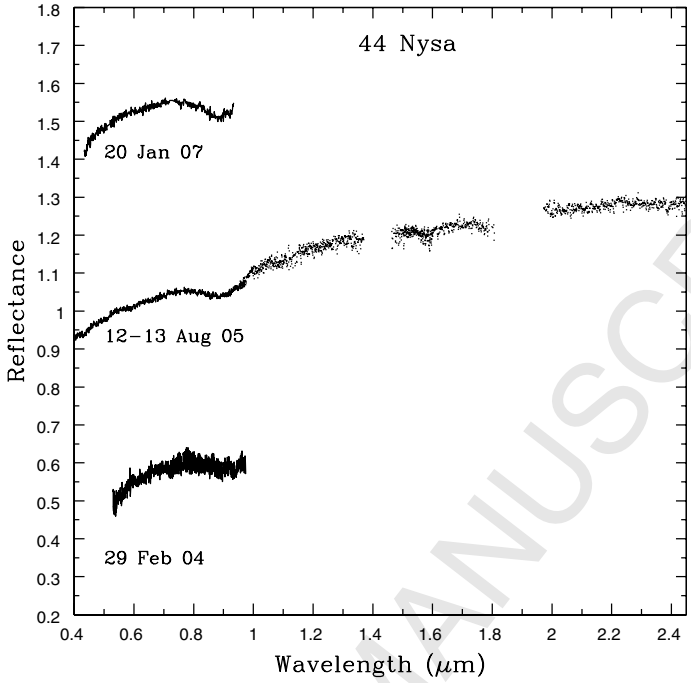

Figure 1:

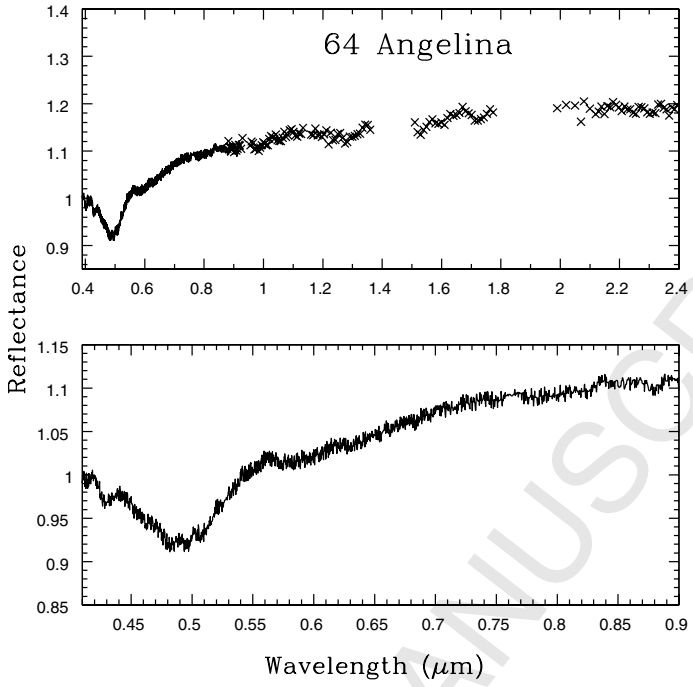

Figure 2:

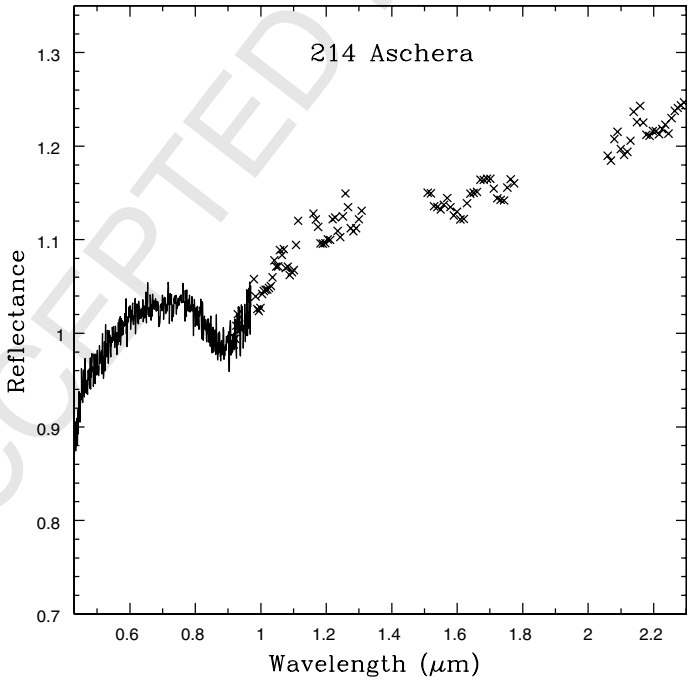

Figure 3:

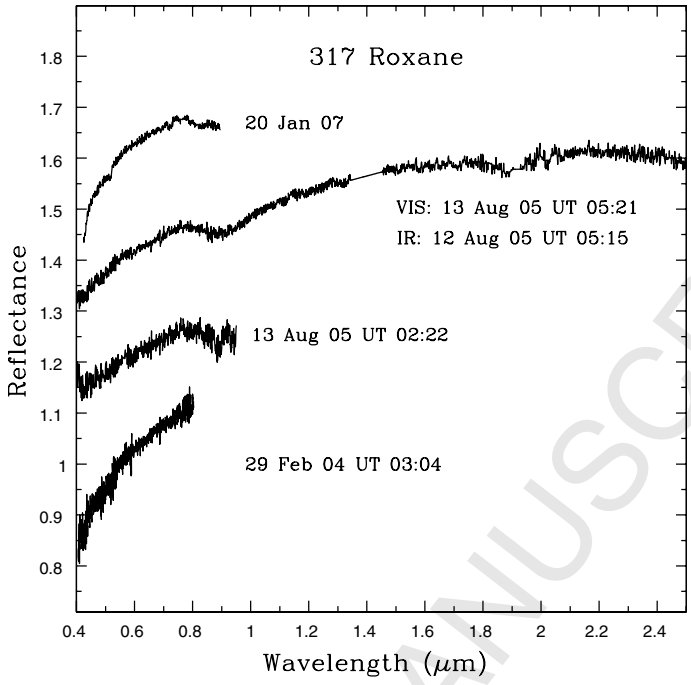

Figure 4:

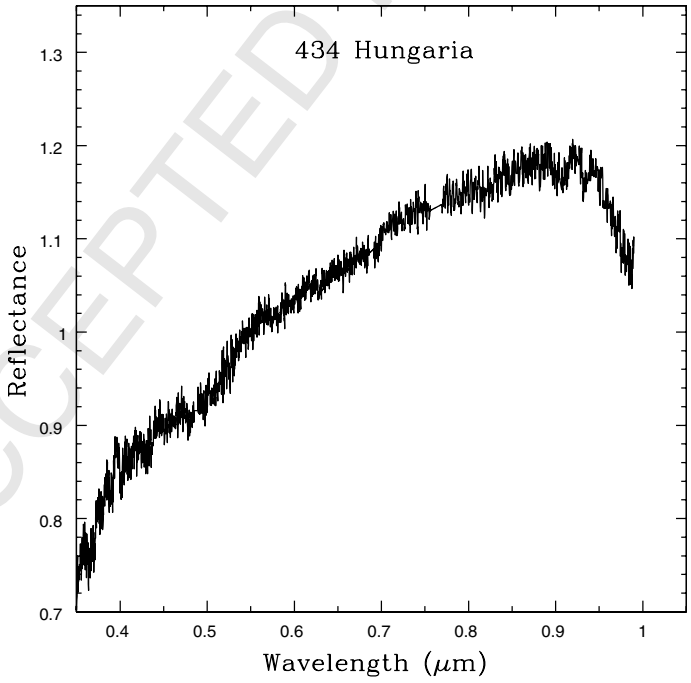

Figure 5:

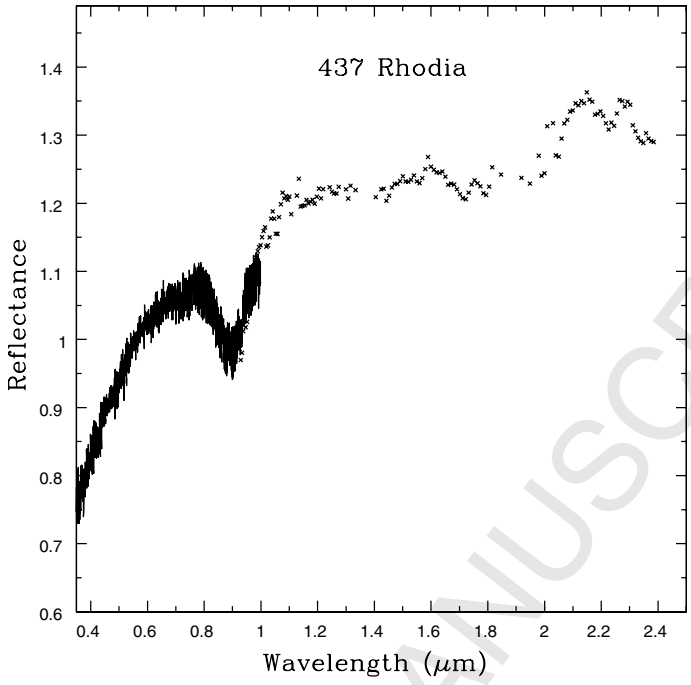

Figure 6:

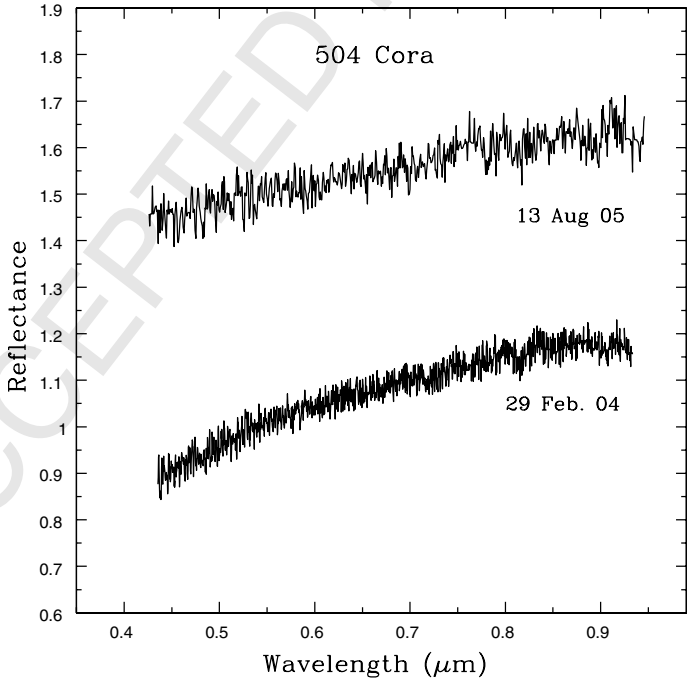

Figure 7:

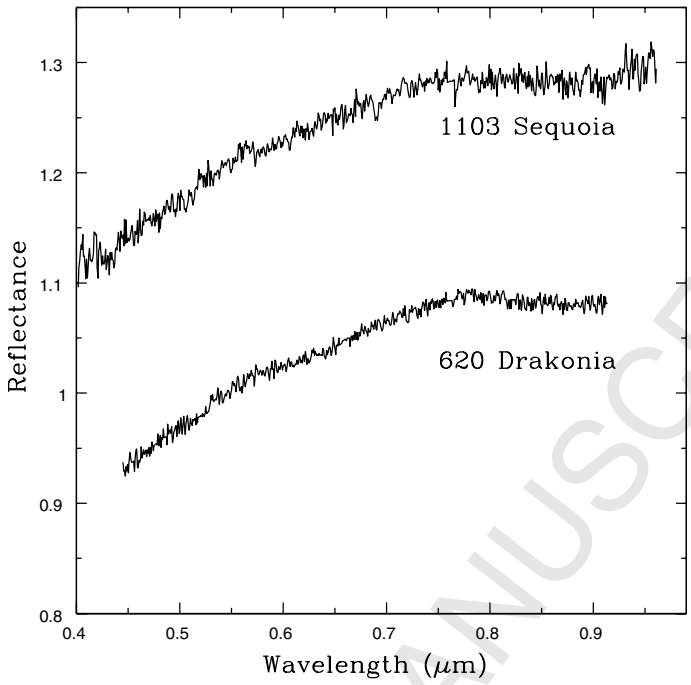

Figure 8:

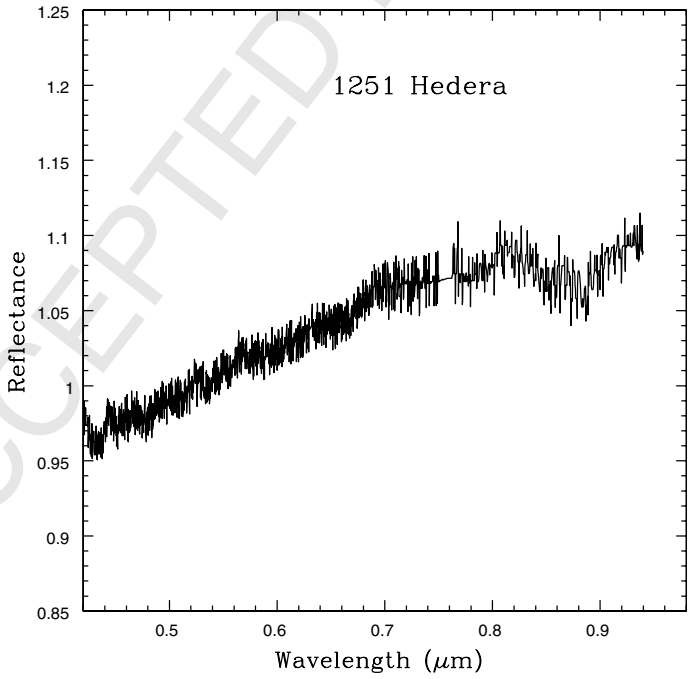

Figure 9:

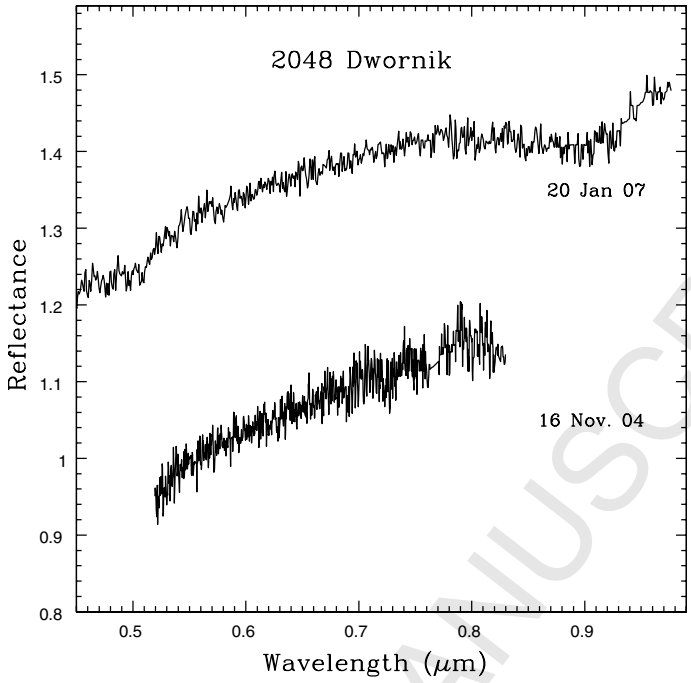

Figure 10:

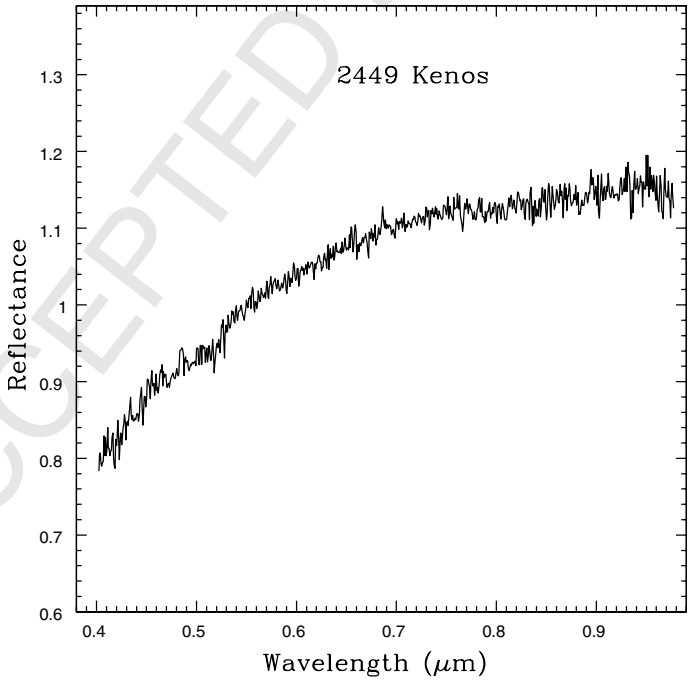

Figure 11:

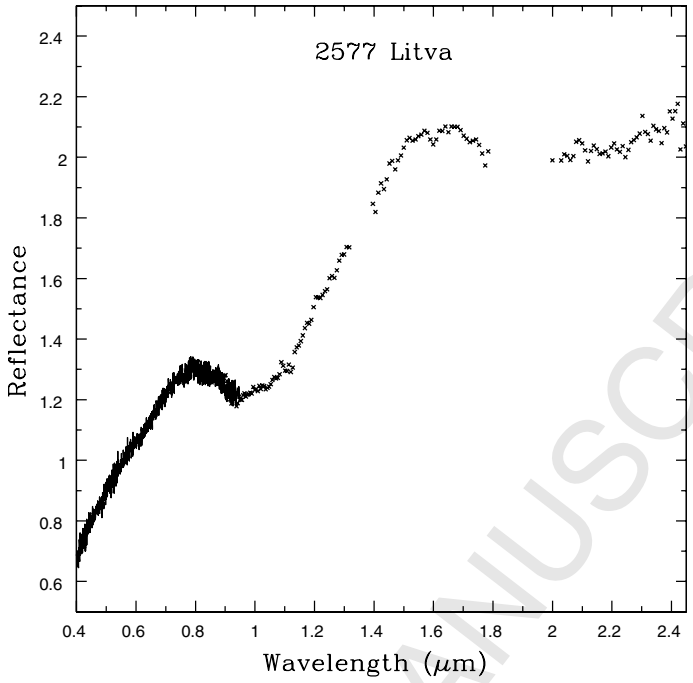

Figure 12:

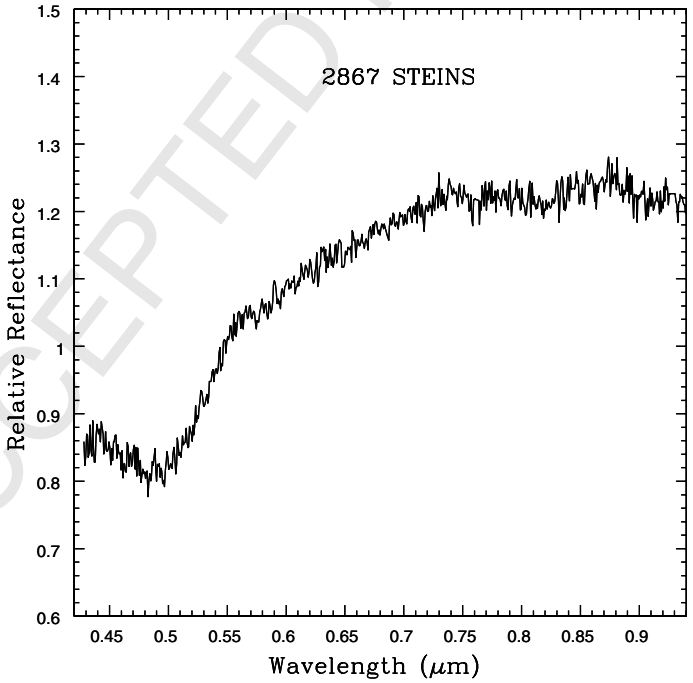

Figure 13:

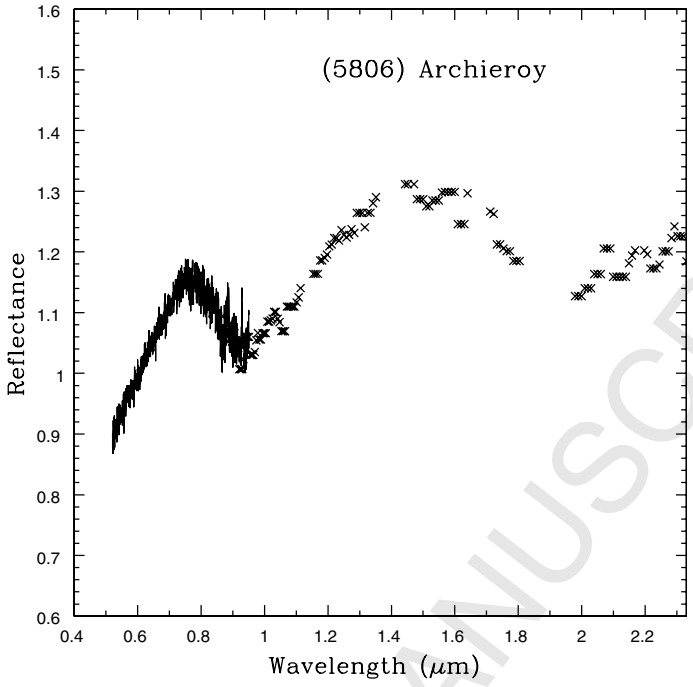

Figure 14:

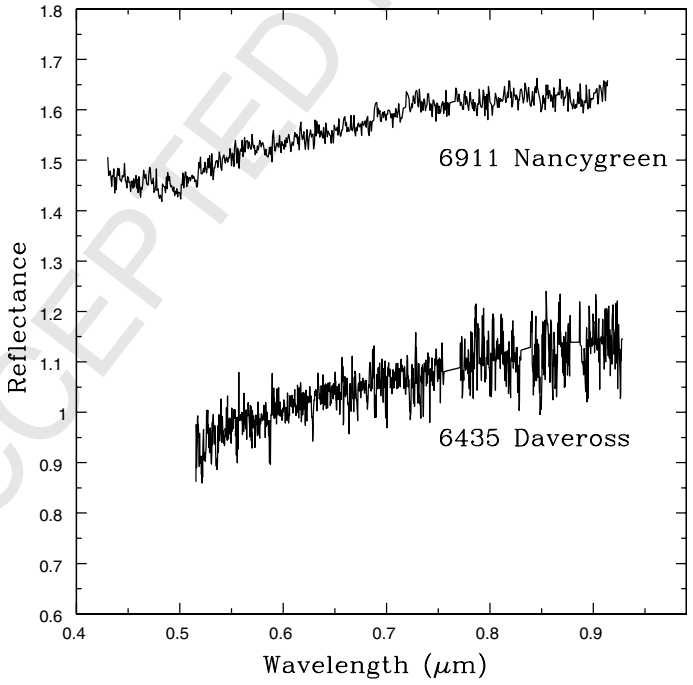

Figure 15:

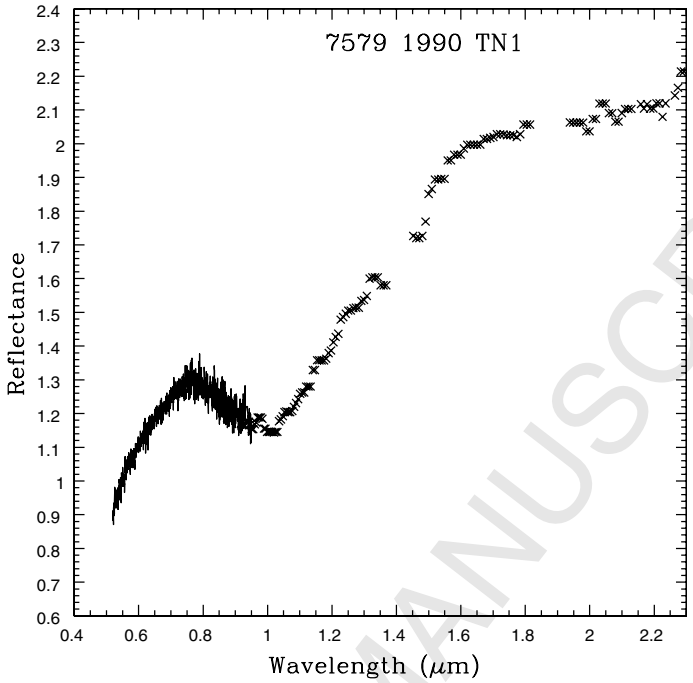

Figure 16:

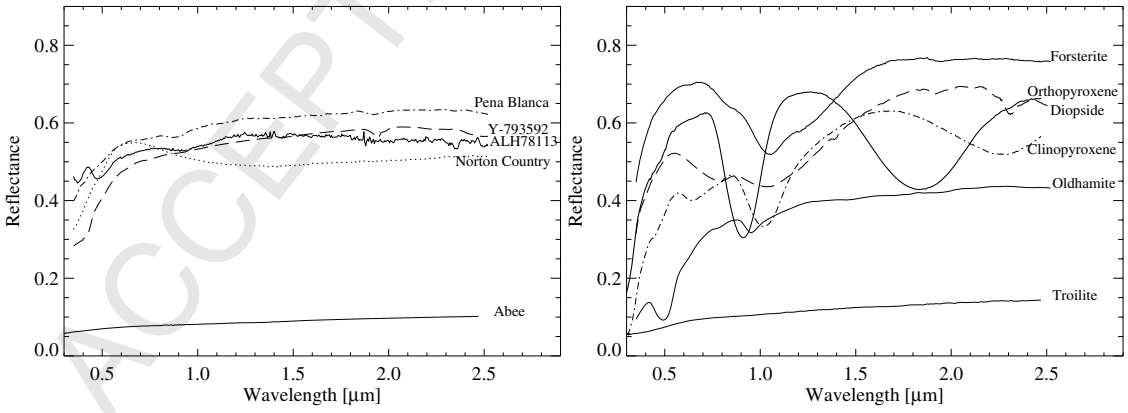

Figure 17:

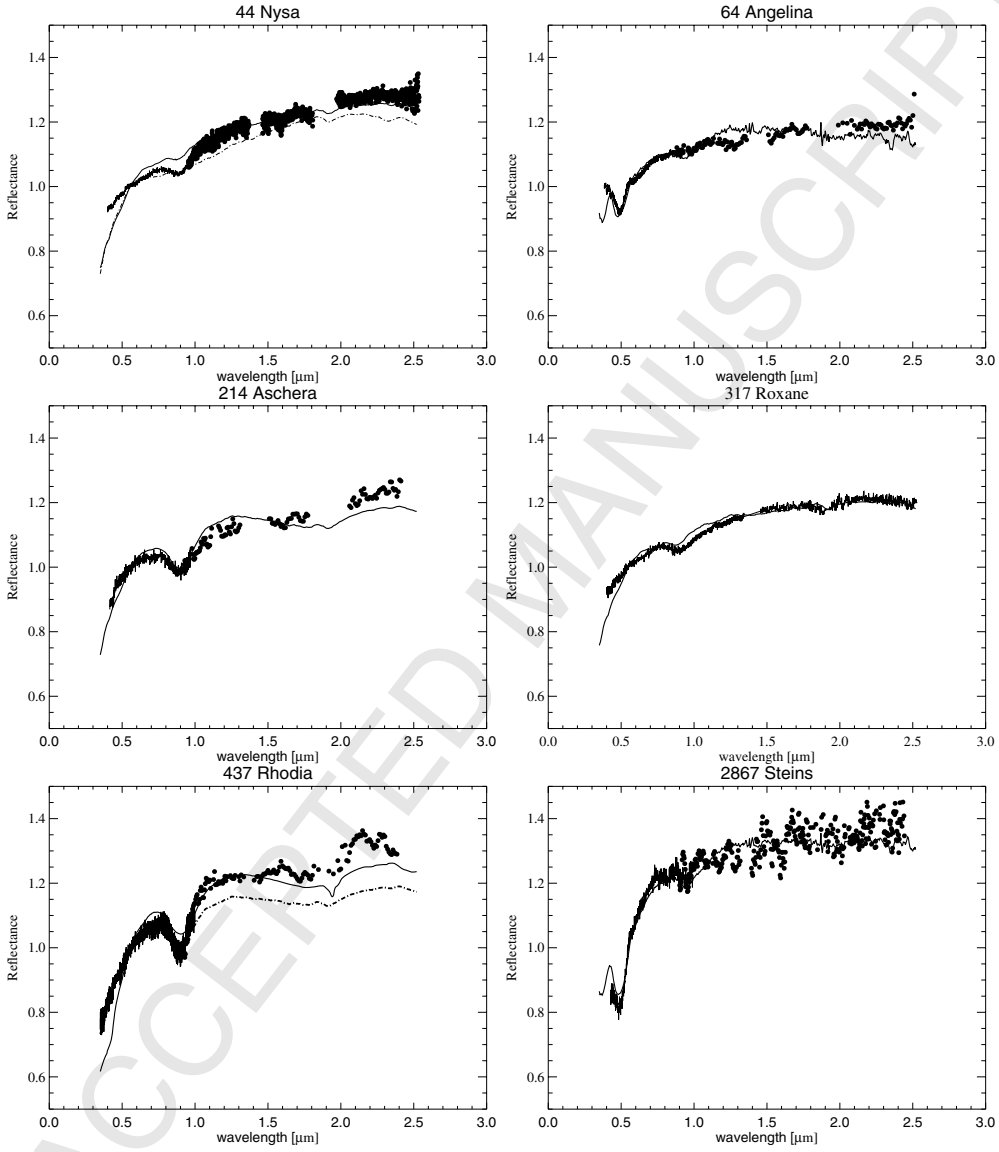

Figure 18:

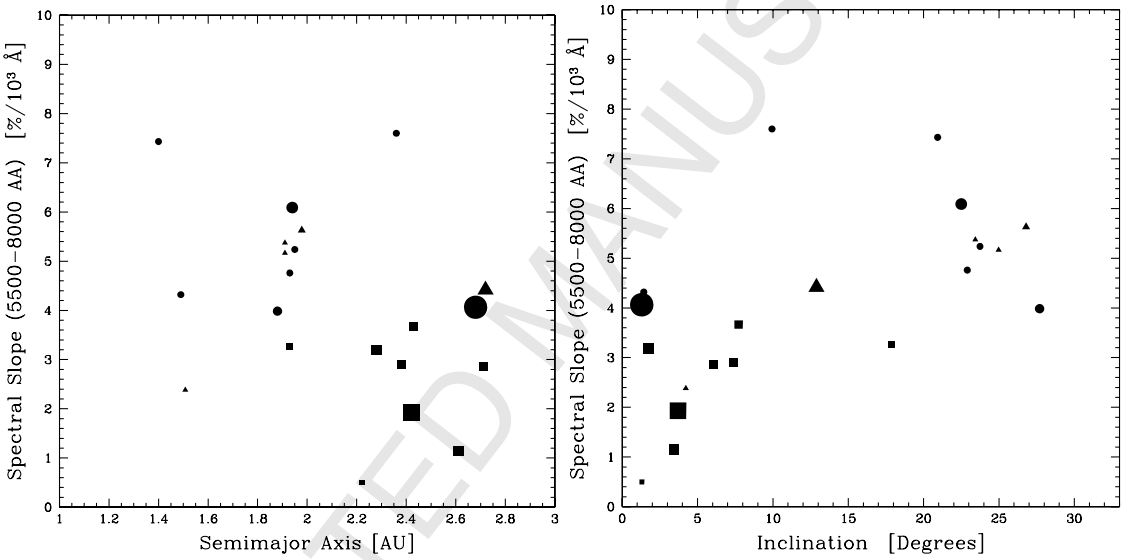

Figure 19: